DALTON
FULL PAPER

Synthesis, spectroscopic and magnetic properties of lanthanide(III) complexes with a chelated imino nitroxide radical

Toshiaki Tsukuda, Takayoshi Suzuki and Sumio Kaizaki *

Department of Chemistry, Graduate School of Science, Osaka University, Toyonaka 560-0043, Japan

Received 19th July 2001, Accepted 28th January 2002
First published as an Advance Article on the web 18th March 2002

The treatment of $[Ln(hfac)_3(H_2O)_2]$ (Ln(III) = Y, Nd–Lu) with IM-2py (2-(2-pyridyl)-4,4,5,5-tetramethyl-1*H*-imidazolyl-1-oxyl) readily gave a series of novel rare earth or lanthanide radical complexes $[Ln(hfac)_3(IM\text{-}2py)]$. The molecular structures of the Sm, Gd, Dy, Er and Yb complexes have been determined to be bicapped trigonal prismatic (*TPRS*) by X-ray diffraction. The magnetic susceptibility data for $[Gd(hfac)_3(IM\text{-}2py)]$ show that the Gd–IM-2py interaction is weakly antiferromagnetic with an exchange coupling constant $J = -3.00\ cm^{-1}$ in contrast to the ferromagnetic interaction in the Gd(III)–nitronyl nitroxide complexes. The n–π* transition of IM-2py is found to shift to lower frequency associated with intensity enhancement and vibronic structure. The luminescence measurement of the Eu(III) and Tb(III) complexes demonstrated energy transfers for IM-2py (SOMO π*) ⟶ Ln(III) (4f) as a result of emission quenching; this depends on the energy gap between the excited levels in Ln(III) and IM-2py. These results reveal that the metal–radical interactions are very weak magnetically but are relatively strong with respect to energy transfer.

Introduction

In the last few years there has been a number of investigations of lanthanide complexes which are potentially applicable to luminescent probes,[1–3] contrast agents in magnetic resonance imaging (MRI),[4] or building blocks in molecular-based magnetic materials.[5] As models for novel magnetic materials in relation to high-temperature superconducting ceramics, much attention has been paid to many heterometal 3d–4f complexes including metal ions such as Cu(II),[6] Ni(II),[7,8a] V(IV)O,[9] Co(III),[10] Zn(II),[11] Cr(III).[8b,12]

On the other hand, instead of paramagnetic metal ions, free nitroxide radical ligands (Scheme 1)[13] have been incorporated

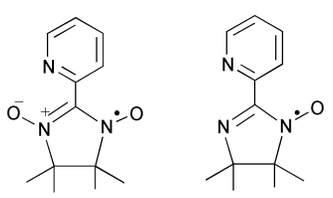

Scheme 1 The nitroxyl and imino nitroxides.

into lanthanide as well as transition metal complexes as building blocks which display a total spin higher than that of the metal ions alone.[14] Among the recent studies of many transition metal nitronyl nitroxide radical complexes,[14a] we have reported the preparation and magneto-optical properties of Cr(III) and Ni(II) NIT-2py complexes (NIT-2py = 2-(2-pyridyl)-4,4,5,5-tetramethyl-1*H*-imidazolyl-3-oxide-1-oxyl).[15] The *β*-diketonato NIT-2py Ni(II) and Cr(III) complexes are found to exhibit a significant intensity enhancement of the formally spin-forbidden d–d bands and newly appeared MLCT components. The spectral behavior was discussed in connection with the observed magnetic coupling constants together with the NMR contact shifts of the β-diketonato methine proton, following two series of six-coordinate octahedral and four-coordinate tetrahedral divalent metal complexes with IM-2py or NIT-2py analogues.[16] There have also been several lanthanide complexes with nitronyl nitroxide radicals. Some of them consist of polymeric chains formed by $Ln(hfac)_3$ moieties (Hhfac = 1,1,1,5,5,5-hexafluoro-2,4-pentanedione) bridged by a nitronyl nitroxide unit through coordination of their oxygen atoms to a Ln atom.[17] Other complexes involve the chelation of a pyridine unit (NIT-2py) forming a six-membered N,O ring.[18] The intramolecular Gd–radical magnetic interactions in these complexes were found to be ferromagnetic.

For an imino nitroxide radical containing pyridyl unit (IM-2py = 2-(2-pyridyl)-4,4,5,5-tetramethyl-1*H*-imidazolyl-1-oxyl)) capable of forming a N,N-five-membered chelate ring (Scheme 1)[19] the intramolecular Ln–radical interaction may exhibit a different type of magnetic interaction between the Ln ion and radical due to the formation of a more planar chelate ring than that formed with NIT-2py.[20a] Transition metal complexes (*e.g.* Mn(II), Co(II), and Ni(II)) containing IM-2py have already been reported[16a,20b] in detail showing ferromagnetic interaction and temperature dependent UV-vis-NIR, spin-forbidden or spin allowed d–d transitions and the dσ or dπ to SOMO π* CT.[16a] A series of complexes of IM-2py with lanthanide(III) ions could provide a clue to gain insight into the ground and lowest excited states in terms of electronic emission and absorption spectroscopy. However, no lanthanide complex containing IM-2py has been reported so far.

In this paper, we describe the preparation and crystal structures of a new series of lanthanide–radical complex containing IM-2py (Scheme 1). The absorption spectroscopy and solid state luminescence spectroscopy are compared with those of the corresponding NIT-2py complexes and the free ligands. The magnetic properties of the Gd complex has also been compared to that of the nitronyl nitroxide radical complexes.

Experimental

Synthesis

All chemicals were reagent grade and used without purification. Lanthanide trichloride hexahydrate and Hhfac were purchased from Wako Pure Chemical Industries Ltd. and Tokyo Chemical Industry Co. Ltd., respectively. The radical ligands NIT-2py[13]

DOI: 10.1039/b106401k

and IM-2py[19] and the starting complexes $[Ln(hfac)_3(H_2O)_2]$[21] and $[Ln(hfac)_3(NIT\text{-}2py)]$[18] were prepared by the literature methods.

$[Ln(hfac)_3(IM\text{-}2py)]$ (Ln = Nd–Lu). $[Ln(hfac)_3(H_2O)_2]$ (1.0 mmol) was suspended in 10 ml CH_2Cl_2. IM-2py (1.37 mmol) in 10 ml CH_2Cl_2 (10 ml) was added to this suspension. After stirring for *ca.* 2 h, a red solution was obtained. The solution was poured into 20 ml of *n*-heptane, and allowed to evaporate slowly. Red-orange crystals were obtained on standing overnight. For the Gd complex the yield is 0.71 g (71%).

The preparative method for $[Nd(hfac)_3(IM\text{-}2py)]$ was slightly altered since the excess volume of ligand resulted in an oily product. $CHCl_3$ was used instead of CH_2Cl_2 and $[Nd(hfac)_3(H_2O)_2]$ (1.0 mmol) was treated with IM-2py (1.0 mmol) by the same method. Yield = 0.52 g (53%).

Measurements

Infrared spectra and UV-vis spectra were recorded on Perkin-Elmer Spectrum-GX FT-IR and Perkin-Elmer Lambda 19 spectrophotometers, respectively. Magnetic susceptibility data were collected at 2000 Oe between 2 and 300 K by using a SQUID susceptometer (MPMS-5S, Quantum Design). Pascal's constants were used to determine the constituent atom diamagnetism.

Luminescence spectra were recorded on a Perkin Elmer LS50B spectrometer at room temperature and 77 K, using an excitation slit width of 10 nm and an emission slit width of 2.5 nm with microcrystalline samples.

X-Ray structural analysis

Red-orange crystals of $[Ln(hfac)_3(IM\text{-}2py)]$ (Ln = Sm, Gd, Dy, Er, Yb) suitable for X-ray crystal analyses were obtained by slowly evaporating a dichloromethane and *n*-heptane solution. Each crystal was mounted in a glass capillary. The X-ray intensities were measured at 23 °C with graphite-monochromated Mo-Kα radiation (λ = 0.71073Å) on a Rigaku AFC-5R or AFC-7R four-circle diffractometer using ω or ω–2θ scan techniques. Final lattice constants were determined by least-squares refinements of the orientation angles of 25 centered reflections in the range $25° < 2\theta < 30°$. Three standard reflections were monitored every 150 reflections and showed no serious decomposition. The intensities collected for $(-h, +k, \pm l)$ octants at $2\theta \leqq 60°$ were corrected for Lorentz-polarization effects, and absorption corrections were made by the Gauss numerical integration method.[22] The structures could be solved reasonably by using direct methods (SIR-92 programs[23a]) and were refined by full matrix least squares procedures (SHELXL-97[23b]). The positions of the hydrogen atoms were fixed at calculated positions and only their isotropic displacement parameters were refined. All calculations were carried out using Crystal Structure software.[24]

CCDC reference numbers 168479–168483.

See http://www.rsc.org/suppdata/dt/b1/b106401k/ for crystallographic data in CIF or other electronic format.

Results and discussion

Preparation and characterization of $[Ln(hfac)_3(IM\text{-}2py)]$

The treatment of $[Ln(hfac)_3(H_2O)_2]$ (with the exception of the Nd complex) with excess amounts of IM-2py in dichloromethane readily gave a red solution of the corresponding $[Ln(hfac)_3(IM\text{-}2py)]$ complexes. Recrystallization was performed from dichloromethane–*n*-heptane solution. For the Nd complex, the use of an excess amount of IM-2py failed to give the desired product, but the reaction with an equimolar amount of IM-2py gave $[Nd^{III}(hfac)_3(IM\text{-}2py)]$, which was recrystallized from chloroform–*n*-hexane. The La, Ce, and Pr complexes, of which the ionic radii is larger than Nd, could not be isolated by this method, since the coordination number of these complexes is apt to be more than eight, *e.g.*, uncharacterized bridging complexes are formed. The products are insoluble in water and dissolve in most organic solvents except aliphatic alkanes, but they readily decompose in methanol, ethanol, and DMSO.

The elemental analyses data and characteristic IR bands for $[Ln(hfac)_3(IM\text{-}2py)]$ are summarized in Table 1. The elemental analyses show that the complexes have a chemical formula consisting of Ln^{3+}, hfac and IM-2py in a 1 : 3 :1 ratio. All of the complexes have almost identical IR spectra with two strong CO stretching bands due to the lower symmetry of $[Ln(hfac)_3(IM\text{-}2py)]$ *versus* $[Ln(hfac)_3(H_2O)_2]$. In addition, these bands shift to higher frequency with increasing Ln atomic number, correlating with the lanthanide contraction as found for the oxalato complexes.[8] Accordingly, it is plausible that the stretching bands of the Y complex are similar to those of the Tm complex, since the ionic radius of the Tm ion is close to that of Y.

Crystallographic studies of $[Ln(hfac)_3(IM\text{-}2py)]$ (Ln = Sm, Gd, Dy, Er, Yb)

For $[Ln(hfac)_3(IM\text{-}2py)]$ (Ln = Sm, Gd, Dy, Er, Yb), red-orange crystals with space group $P2_1/n$ were formed by recrystallization from dichloromethane–*n*-heptane solution. Crystallographic data for each complex are listed in Table 2. The molecular structure of $[Gd(hfac)_3(IM\text{-}2py)]$ is illustrated in Fig. 1. The Gd atom

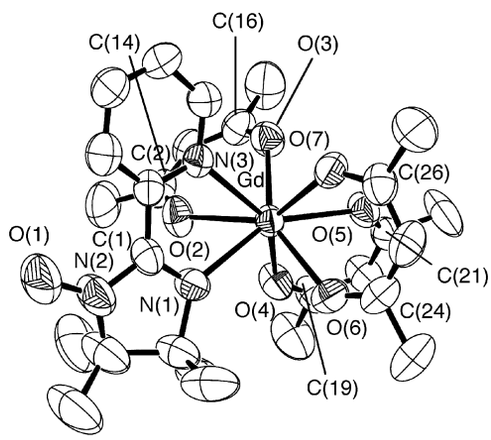

Fig. 1 Molecular structure of $[Gd(hfac)_3(IM\text{-}2py)]$, showing 50% probability ellipsoids (F atoms are omitted).

of $[Gd(hfac)_3(IM\text{-}2py)]$ is eight-coordinated with three bidentate hfac ligands and one bidentate IM-2py ligand. Selected bond lengths and angles are also shown in Table 3.

The N(2)–O(1) bond length (1.282(7) Å) in the Gd complex is slightly longer than that of the other transition metal complexes containing IM-2py (1.265–1.271 Å),[16a] but significantly shorter than that of an average N–O single bond (1.41 Å). This fact indicates the existence of a radical unpaired spin upon complexation. In view of the torsion angles, the planes N(1), C(1), N(2), O(1) and N(1), C(1), C(2), O(1) are nearly planar, with the SOMO(π*) orbital expanding to the ligated N(3) atom. The Gd–O(hfac) bond lengths can be classified into two groups. (a) Those with Gd–O bond lengths (Gd–O(3), Gd–O(4), Gd–O(6) and Gd–O(7)) ranging from 2.315(5) Å to 2.367(5) Å and (b) those with bond lengths of 2.401(4) Å (Gd–O(2)) and 2.417(4) Å (Gd–O(5)). The bond lengths in the second group (b) are longer than those in the first group (a). These bond lengths are similar to those (2.33–2.35 Å) found for $[Gd(hfac)_3Cu(salen)]$[6a] (salen = *N*,*N*′-ethylenebis(salicylidene)diaminate). The Gd–N(3) (pyridine-N) bond length (2.553(4) Å) is comparable with the Gd–N(py) bond length for the eight-coordinate complex $[Gd(hfac)_3(NIT\text{-}2py)]$[18] (2.614(9) Å). The

Table 1 Elemental analysis for the complexes (calculated values are given in parentheses)

	C	H	N	ν(C=O)/cm^{-1}
[Y(hfac)$_3$(IM-2py)]	35.01 (34.93)	1.94 (2.06)	4.66 (4.53)	1651, 1668
[[Nd(hfac)$_3$(IM-2py)]	32.73 (32.97)	1.84 (1.95)	4.47 (4.27)	1648, 1664
[Sm(hfac)$_3$(IM-2py)]	32.95 (32.76)	1.90 (1.93)	4.66 (4.25)	1648, 1664
[Eu(hfac)$_3$(IM-2py)]	32.57 (32.71)	1.83 (1.93)	4.53 (4.24)	1648, 1665
[Gd(hfac)$_3$(IM-2py)]	32.89 (32.54)	1.86 (1.92)	4.45 (4.22)	1649, 1666
[Tb(hfac)$_3$(IM-2py)]	32.14 (32.48)	1.78 (1.92)	4.49 (4.21)	1649, 1667
[Dy(hfac)$_3$(IM-2py)]	32.74 (32.37)	1.85 (1.91)	4.43 (4.19)	1649, 1667
[Ho(hfac)$_3$(IM-2py)]	32.53 (32.29)	1.82 (1.91)	4.33 (4.18)	1649, 1667
[Er(hfac)$_3$(IM-2py)]	32.41 (32.21)	1.82 (1.90)	4.38 (4.17)	1650, 1668
[Tm(hfac)$_3$(IM-2py)]	32.23 (32.16)	1.96 (1.90)	4.65 (4.17)	1651, 1668
[Yb(hfac)$_3$(IM-2py)]	32.08 (32.03)	1.82 (1.89)	4.35 (4.15)	1652, 1669
[Lu(hfac)$_3$(IM-2py)]	32.12 (31.97)	1.81 (1.89)	4.27 (4.14)	1652, 1670

Table 2 Crystallographic data for [Ln(hfac)$_3$(IM-2py)][a]

	Ln = Sm	Gd	Dy	Er	Yb
Formula	$C_{27}H_{19}O_7N_3F_{18}Sm$	$C_{27}H_{19}O_7N_3F_{18}Gd$	$C_{27}H_{19}O_7N_3F_{18}Dy$	$C_{27}H_{19}O_7N_3F_{18}Er$	$C_{27}H_{19}O_7N_3F_{18}Yb$
M	989.79	996.70	1001.93	1006.69	1012.47
a/Å	12.258(5)	12.183(1)	12.139(3)	12.101(1)	12.052(4)
b/Å	31.560(6)	31.601(3)	31.568(7)	31.582(4)	31.568(6)
c/Å	9.619(5)	9.588(2)	9.572(3)	9.554(1)	9.546(5)
β/°	98.72(4)	98.56(1)	98.54(2)	98.48(1)	98.37(3)
V/Å^3	3678.2(2)	3650.2(7)	3627.2(1)	3611.4(7)	3593.3(2)
$R1$	0.0435	0.0424	0.0479	0.0487	0.0583
$wR2$	0.1158	0.1122	0.1330	0.1261	0.1498
GOF	1.005	0.968	1.004	0.948	0.967

[a] Space group $P2_1/n$, monoclinic and $Z = 4$ for all compounds.

Table 3 Selected bond distances (Å), bond angles (°) and torsion angles (°) for [Gd(hfac)$_3$(IM-2py)]

Gd–O(2)	2.401(4)	O(2)–C(14)	1.230(7)
Gd–O(3)	2.346(4)	O(3)–C(16)	1.268(7)
Gd–O(4)	2.328(4)	O(4)–C(19)	1.243(7)
Gd–O(5)	2.417(4)	O(5)–C(21)	1.222(7)
Gd–O(6)	2.354(4)	O(6)–C(24)	1.251(8)
Gd–O(7)	2.349(4)	O(7)–C(26)	1.237(7)
Gd–N(1)	2.540(5)	N(2)–O(1)	1.282(7)
Gd–N(3)	2.553(4)	N(1)–C(1)	1.287(7)
O(2)–Gd–O(3)	72.00(15)	O(2)–Gd–O(4)	74.78(15)
O(2)–Gd–O(5)	128.64(15)	O(2)–Gd–O(6)	136.87(15)
O(2)–Gd–O(7)	142.03(14)	O(2)–Gd–N(1)	70.06(15)
O(2)–Gd–N(3)	72.89(15)	O(3)–Gd–O(4)	93.78(15)
O(3)–Gd–O(5)	72.35(15)	O(3)–Gd–O(6)	146.68(15)
O(3)–Gd–O(7)	90.83(14)	O(3)–Gd–N(1)	136.63(15)
O(3)–Gd–N(3)	84.98(15)	O(4)–Gd–O(5)	72.00(13)
O(4)–Gd–O(6)	82.39(15)	O(4)–Gd–O(7)	141.57(14)
O(4)–Gd–N(1)	95.86(14)	O(4)–Gd–N(3)	146.36(14)
O(5)–Gd–O(6)	75.03(15)	O(5)–Gd–O(7)	73.21(14)
O(5)–Gd–N(1)	150.35(16)	O(5)–Gd–N(3)	137.83(14)
O(6)–Gd–O(7)	73.31(14)	O(6)–Gd–N(1)	76.62(16)
O(6)–Gd–N(3)	115.98(15)	O(7)–Gd–N(1)	106.58(15)
O(7)–Gd–N(3)	72.05(13)	N(1)–Gd–N(3)	64.43(14)
N(1)–C(1)–C(2)–N(3)	8.6(8)		
N(1)–C(1)–N(2)–O(1)	2.7(7)		

Gd–N(1) (imidazole-N) bond length (2.540(5) Å) is similar to the Gd–N(3) length.

The other lanthanide atoms of [Ln(hfac)$_3$(IM-2py)] have a similar coordination geometry to each other. The Ln–O(hfac) bond lengths of all these complexes can also be classified into two groups. For example, in the Yb complex, one group ranges from 2.245(5) Å to 2.289(6) Å and the other from 2.342(6) Å to 2.345(5) Å. Additionally, the Ln–N(1) and Ln–N(3) bond lengths are similar to each other. The Yb–N bond lengths are 2.480(6) (Yb–N(1)) and 2.480(5) (Yb–N(3)).

The N_2O_6 eight-coordinate geometries are square antiprism (*SAPR*), dodecahedral (*DD*), and bicapped trigonal prism (*TPRS*) (Scheme 2). They were examined by using the semi-quantitative method of polytopal analysis.[25] The δ and φ values are summarized in Table 4. In [Sm(hfac)$_3$(IM-2py)] the δ_1 and δ_2 values showing planarity of the squares are 29.70° and 8.50°, respectively. The δ_1 values are relatively large, but δ_2 are still small. The φ_1 and φ_2 values are 12.49° and 7.69°, respectively. These values are fairly close to the angle (14.1°) of the ideal *TPRS* polyhedron. Thus, the most reasonable geometry around the Sm atom is *TPRS*. All the complexes have an almost *TPRS* geometry. Two oxygen atoms with longer Ln–O(hfac) bond lengths than the others are located in the square bicapped vertices. The δ_2 value tends to increase from Sm to Yb, though the change is not always constant throughout the series. Both of the φ values decrease almost in this order. Therefore, it is suggested that the present complexes become slightly closer to *DD* than *TPRS* with decreasing ionic radii of the central Ln ion, in other words, they are on a geometric pathway to *DD* from *TPRS*.

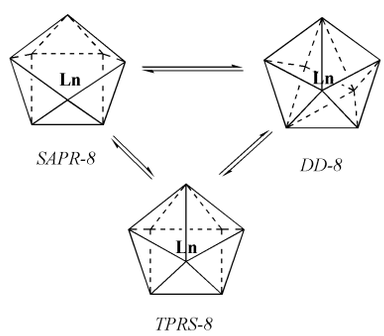

Scheme 2

Magnetic properties of [Gd(hfac)$_3$(IM-2py)]

The variable temperature magnetic susceptibilities of [Gd(hfac)$_3$(IM-2py)] are shown in the form of $\chi_M T$ *versus* T plots in Fig. 2. Since the ground state of Gd(III) ($^8S_{7/2}$) is orbitally non-degenerate and well separated from the excited state,

Table 4 δ (°) and φ (°) values for [Ln(hfac)$_3$(IM-2py)]

	TPRS-8	Sm	Gd	Dy	Er	Yb	*DD*-8
δ_1: O(2) [O(3) O(4)] O(5)[a]	21.8	29.70	28.63	28.85	28.72	28.92	29.5
δ_2: N(3) [N(1) O(7)] O(6)[a]	0.0	8.50	8.28	10.04	10.83	12.21	29.5
δ_3: N(3) [O(3) O(7)] O(5)[a]	48.2	37.04	37.02	36.49	36.07	35.54	29.5
δ_4: O(2) [N(1) O(4)] O(6)[a]	48.2	38.02	38.18	37.01	36.71	36.93	29.5
φ_1: O(2)–N(3)–O(4)–O(7)[b]	14.1	12.49	12.25	11.08	10.40	9.85	0.0
φ_2: O(5)–N(6)–O(3)–N(1)[b]	14.1	7.69	8.14	7.21	6.89	6.57	0.0

[a] A [B C] D is the dihedral angle between the ABC plane and the BCD plane. [b] A–B–C–D is the dihedral angle between the (AB)CD plane and the AB(CD) plane, where (AB) is the center of A and B.

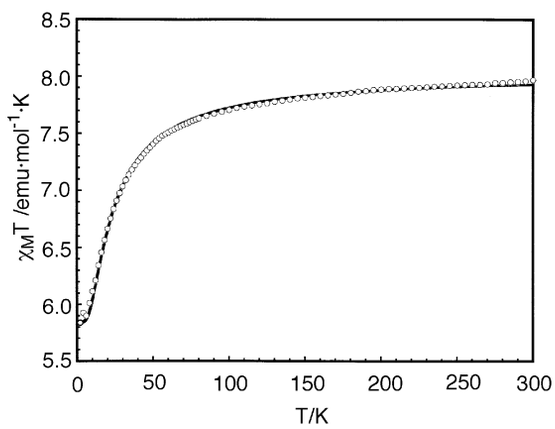

Fig. 2 Temperature dependence of $\chi_M T$ in the 4.2–300 K range for [Gd(hfac)$_3$(IM-2py)]. The solid line is calculated with the parameters reported in the text.

Gd(III) exhibits simple single ion magnetic properties. The observed $\chi_M T$ value (7.99 emu mol^{-1} K) at room temperature is a little smaller than the expected value for uncoupled Gd(III) and IM-2py (calculated value 8.12 emu mol^{-1} K). The $\chi_M T$ value of this complex slightly decreases upon lowering the temperature, and then below 100 K, a drastic decrease appears. As the crystal structure showed that there is a discrete molecule containing one gadolinium ion and one imino nitroxide with no intermolecular interactions, the magnetic data were analyzed on the assumption of an interaction between the IM-2py spin and 4f spins. The usual van Vleck equation for this type of dimer was derived by using the isotropic Hamiltonian $H = -2JS_1 \cdot S_2$.[18] A good fit to the experimental data is obtained for $J = -3.00$ cm^{-1} and $g = 1.97$ with the agreement factor $R = \Sigma[(\chi_M)_{obs} - (\chi_M)_{calc}]^2/\Sigma(\chi_M)_{obs}^2$ equal to 5.66×10^{-5}.

It is noted that the magnetic interaction for the present complex is uncommonly antiferomagnetic.[26] It is found that the interaction between Gd(III) and NIT type radicals is generally ferromagnetic; for the monodentate radical complex [Gd(hfac)$_3$(NIT-iPr)(H$_2$O)][17a] $J = 0.33$ cm^{-1} and for the bidentate chelate type radical complex [Gd(hfac)$_3$(NIT-2py)][18] $J = 1.51$ cm^{-1}. The ferromagnetic interaction between the lanthanide ion and the paramagnetic NIT radical ligands is claimed to involve unpaired electron transfer of the organic ligands into the empty 5d and 6s orbitals of the metal, resulting in the parallel alignment of the 4f and 5d, 6s electrons according to Hund's rule.[27] Thus in this mechanism the extent of the ferromagnetic interaction may depend on the overlap between the SOMO π* orbital of the nitroxide and the 5d and/or 6s orbitals of the metal as has been similarly proposed for Gd(III)–Cu(II).[28] On the basis of the fact that the Gd–NIT-2py complex is ferromagnetic, the electron transfer integral $\beta_{5d\text{–}SOMO\ \pi^*}$ or the overlap of the 5d, 6s orbital with the NIT-2py SOMO π* orbital is considered to be appreciable. Conversely, the IM-2py SOMO π* orbital is predicted to be less overlapped or orthogonal to the 5d, 6s orbital. This is analogous to the case of the Ni(II) complexes, where planar IM-2py chelation makes the IM-2py SOMO π* orthogonal with the 3d orbital in contrast to the nonplanar NIT-2py one.[16,20b] Since the observed magnetic coupling constant J_{obs} represents the sum of the antiferrromagnetic one J_{AF} and ferromagnetic one J_F ($J_{obs} = J_{AF} + J_F$), the decreasing overlap of 5d, 6s with the IM-2py SOMO π* orbital results in a decrease in the ferromagnetic contribution to J_{obs} or the antiferromagnetic interaction. This is interesting in relation to the recent finding that the configurations 4f^7 to 4f^{10} and 4f^1 to 4f^5 are ferromagnetic and antiferromagnetic, respectively, for the radical Ln(III) complexes. Our research extending to the other Ln(III) complexes is now in progress.

Spectral properties of [Ln (hfac)$_3$(IM-2py)]

(a) Absorption spectra of [Ln(hfac)$_3$(IM-2py)]. Absorption spectra of [Sm(hfac)$_3$(IM-2py)] and [Yb(hfac)$_3$(IM-2py)] are shown together with that of IM-2py in Fig. 3. The numerical data are summarized in Table 5. The spectral change with increasing ratio of [Y(hfac)$_3$(H$_2$O)] and IM2-py are shown in Fig. 4. The complexation equilibrium is expected to follow the expression:

$$[Y(hfac)_3(H_2O)_2] + \text{IM-2py} \rightleftharpoons [Y(hfac)_3(\text{IM-2py})] + 2H_2O$$

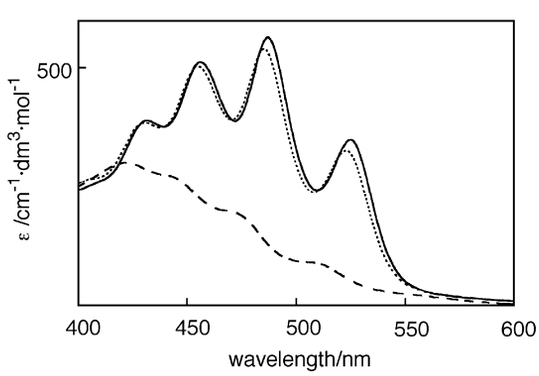

Fig. 3 Absorption spectra of [Sm(hfac)$_3$(IM-2py)] (—), [Yb(hfac)$_3$(IM-2py)] (···) and IM-2py (---).

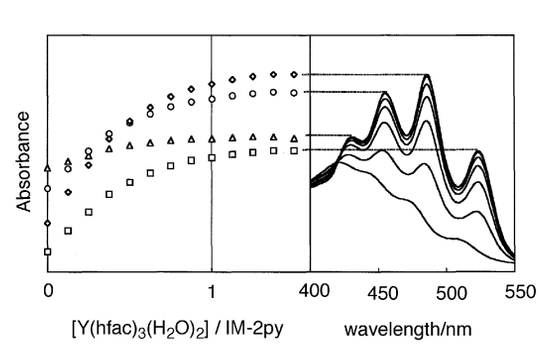

Fig. 4 The change in UV-VIS absorption spectrum with the ratio [Y(hfac)$_3$(H$_2$O)$_2$] : IM-2py increasing in acetonitrile (□, 524 nm; ◇, 486 nm; ○, 451 nm; △, 432 nm).

Table 5 λ_{max} (nm) of absorption spectra in $CHCl_3$ for the IM-2py ligand and the complexes[a]

	IM-2py	[Sm(hfac)$_3$(IM-2py)]	[Yb(hfac)$_3$(IM-2py)]
n–π* transition	420 (299)	430 (384)	431 (389)
(intraligand)	444^{sh} (269)	455 (504)	456 (512)
	475^{sh} (188)	485 (541)	487 (566)
	510^{sh} (88)	523 (326)	524 (348)
f–f transition			978 (5)
			955 (2)
			931 (2)

[a] Molar absorption constants are given in parentheses.

The maximum absorption intensities of the n–π* band become larger until the ratio increases to *ca.* 1 : 1. When the ratio is more than unity, the spectral change is negligible. Thus, the stabilization constant of this complexation is large, and a major amount of [Ln(hfac)$_3$(IM-2py)] exists as a stable species in solution.

By comparison with the intraligand n–π* transition of IM-2py in the region from 19 × 10^3 cm^{-1} to 24 × 10^3 cm^{-1}, the absorption bands of [Ln(hfac)$_3$(IM-2py)] in the corresponding region are assigned to the intraligand n–π* transition, though they are shifted to lower frequency. The lower energy shift of the n–π* transition in the lanthanide–radical complex have been also observed in [Gd(NITBzIMH)$_2$(NO$_3$)] [NITBzIMH = 2-(2-benzimidazolyl)-4,4,5,5-tetramethyl-1*H*-imidazolyl-1-oxyl 3-oxide].[29] The vibrational structure of the complex is observed more clearly than that of the free IM-2py ligand. The molar absorption coefficients of the complexes are much larger than those of free IM-2py. The spectral behavior of the n–π* absorption bands are almost unchanged from one Ln–IM-2py complex to another, although a slight shift to lower frequency is seen with decreasing ionic radius of the central Ln ion. Two causes of this behavior may be considered: (i) as a result of chelation the radical SOMO π* energy level are slightly stabilized due to an increase in planarity between the N=C–N=O moiety and the pyridine ring leading to expansion of the conjugated system; (ii) the electronic state of the ligand is considerably affected by coordination bond formation with lanthanide(III) ions as found for Schiff base complexes.[30] We have also observed a red shift in the n–π* absorption bands for the diamagnetic Co(III) complexes[31] bearing NIT-*n*py and IM-*n*py (3- or 4-pyridyl substituted NIT and IM) as unidentate ligands through pyridyl coordination.

(b) Emission spectra of [Ln(hfac)$_3$(IM-2py)]. It is generally found that characteristic sharp luminescence is observed for Eu(III) and Tb(III) complexes.[32,33] Actually, the microcrystalline samples of the nonradical complexes [Eu(hfac)$_3$(bpy)] and [Tb(hfac)$_3$(bpy)] show sharp emission bands at room temperature when they are irradiated at the 4f–4f transitions; 465 nm ($^7F_0 \longrightarrow {}^5D_2$ for Eu(III)) or 488 nm ($^7F_6 \longrightarrow {}^5D_4$ for Tb(III)), respectively (Fig. 5). However, neither [Eu(hfac)$_3$(NIT-2py)] nor [Tb(hfac)$_3$(NIT-2py)] gives emission bands. That is, efficient quenching of the luminescence occurs, resulting from the resonance between the Ln(III) excited levels and the broad absorption band of NIT-2py, since the n–π* absorption band envelope for the NIT-2py ligand overlaps with the energy level of emission departure for Eu(III) and Tb(III) ($^5D_0$ for Eu(III) and $^5D_4$ for Tb(III)) as shown in Fig. 5.

In the IM-2py complexes, [Tb(hfac)$_3$(IM-2py)] and [Eu(hfac)$_3$(IM-2py)] exhibit no emission bands due to quenching insofar as the wavelength of the irradiation is 465 nm as found for the NIT-2py complexes. No emission with excitation of 465 nm is due to no occurrence of energy transfer from IM-2py (n–π*) to Eu(III) ($^5D_0$) (Fig. 6).

When the excitation wavelength is 222 nm, presumably corresponding to CT due to the coordinated hfac ligand, sharp

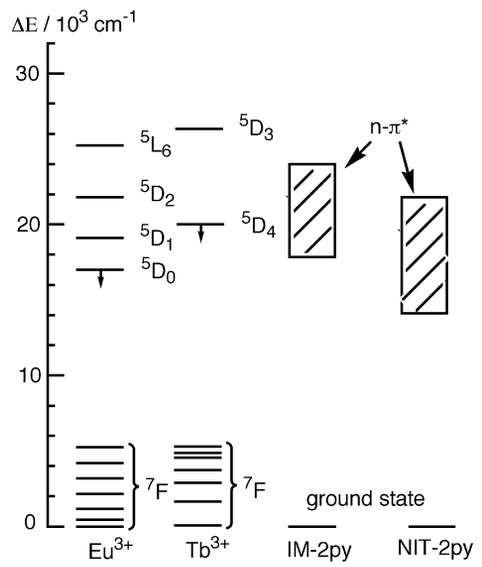

Fig. 5 Energy level diagram showing 4f states of Ln(III) and ligand levels of NIT-2py and IM-2py. The arrows indicate emission levels of Eu(III) and Tb(III).

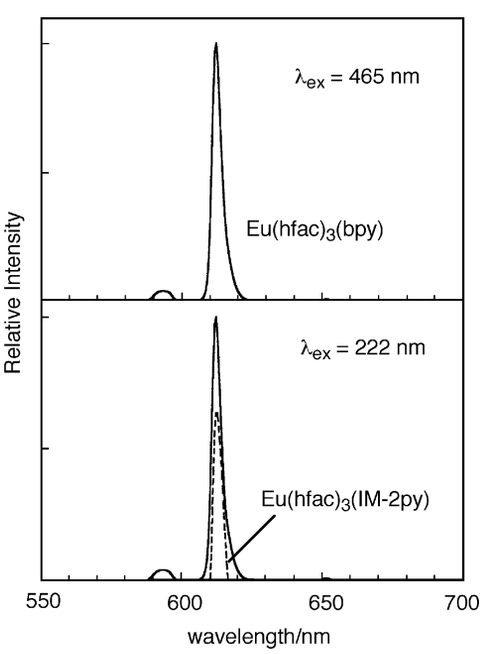

Fig. 6 Emission spectra of [Eu(hfac)$_3$(bpy)] (—) and [Eu(hfac)$_3$(IM-2py)] (· · ·) in the solid state.

emission bands are observed for the Eu(III) but not for the Tb(III) complex at room temperature (Fig. 6). As compared with NIT-2py, the n–π* absorption band envelope for the IM-2py ligand does not overlap with the luminescent energy level of

Eu(III) ($^5D_0$), but overlaps with that of Tb(III) ($^5D_4$); the molar absorption coefficients ε being *ca.* 10 and 300 $dm^3\ cm^{-1}\ mol^{-1}$ at 580 nm and 500 nm, respectively. This overlap prevents effective quenching.

Conclusion

A new series of the discrete Ln(III)–IM-2py complexes were readily prepared and are stable in solution and in the solid state. Two types of metal–metal interaction between Ln(III) and the IM-2py ligand have been found; (i) the magnetic interactions between Gd(III) and IM-2py are weakly antiferromagnetic in contrast to the ferromagnetic interaction between Gd(III) and nitronyl nitroxides and (ii) the interactions in the excited state are relatively strong in view of both the red shift and/or intensity enhancement with vibronic structure in the n–π* intraligand transition of IM-2py and the emission quenching behavior.

References

1 J.-C. G. Bünzli, *in Lanthanide Probes in Life, Chemical and Earth Sciences, Theory and Practice*, Elsevier, New York 1989, p. 219.
2 R. D. Archer, H. Chen and L. C. Thompson, *Inorg. Chem.*, 1998, **37**, 2089.
3 L. Prodi, S. Pivari, F. Bolletta, M. Hissler and R. Ziessel, *Eur. J. Inorg. Chem.*, 1998, 1959.
4 R. B. Lauffer, *Chem. Rev.*, 1987, **87**, 901.
5 (*a*) O. Kahn, *Adv. Inorg. Chem.*, 1995, **43**, 179; (*b*) C. Benelli, A. J. Blake, P. E. Y. Milne, J. M. Rawson and R. E. P. Winpenny, *Chem. Eur. J.*, 1995, **1**, 614.
6 (*a*) I. Ramade, O. Kahn, Y. Jeannin and F. Robert, *Inorg. Chem.*, 1997, **36**, 930; (*b*) J.-P. Costes, F. Dahan and A. Dupuis, *Inorg. Chem.*, 2000, **39**, 165; (*c*) J.-P. Costes, F. Dahan, A. Dupuis and J.-P. Laurent, *Inorg. Chem.*, 2000, **39**, 169; (*d*) J.-P. Costes, F. Dahan and A. Dupuis, *Inorg. Chem.*, 2000, **39**, 5994.
7 (*a*) J.-P. Costes, F. Dahan, A. Dupuis and J.-P. Laurent, *Inorg. Chem.*, 1997, **36**, 4284; (*b*) Y. Yukawa, S. Igarashi, A. Yamano and S. Sato, *Chem. Commun.*, 1997, 711; (*c*) S. J. Archibald, A. J. Blake, S. Parsons, M. Schröder and R. E. P. Winpenny, *J. Chem. Soc., Dalton Trans.*, 1997, 173.
8 (*a*) T. Sanada, T. Suzuki and S. Kaizaki, *J. Chem. Soc., Dalton Trans.*, 1998, 959; (*b*) T. Sanada, T. Suzuki, T. Yoshida and S. Kaizaki, *Inorg. Chem.*, 1998, **37**, 4712; (*c*) Md. A. Subhan, T. Suzuki and S. Kaizaki, *J. Chem. Soc., Dalton Trans.*, 2001, 492.
9 (*a*) J.-P. Costes, A. Dupuis and J.-P. Laurent, *J. Chem. Soc., Dalton Trans.*, 1998, 735; (*b*) J.-P. Costes, F. Dahan, B. Donnadieu, J. G. Tojal and J.-P. Laurent, *Eur. J. Inorg. Chem.*, 2001, 363.
10 (*a*) S. Rigault, C. Piguet, G. Bernardinelli and G. Hopfgartner, *Angew. Chem., Int. Ed.*, 1998, **37**, 169; (*b*) S. Rigault, C. Piguet and J.-C. G. Bünzli, *J. Chem. Soc., Dalton Trans.*, 2000, 2045.
11 (*a*) C. Piguet, J.-C. G. Bünzli, G. Bernardinelli, G. Hopfgartner, S. Petoud and O. Schaad, *J. Am. Chem. Soc.*, 1996, **118**, 6681; (*b*) C. Edder, C. Piguet, J.-C. G. Bünzli and G. Hopfgartner, *J. Chem. Soc., Dalton Trans.*, 1997, 4657.
12 (*a*) N. Sakagami, M. Tsunekawa, T. Konno and K. Okamoto, *Chem. Lett.*, 1997, 575; (*b*) N. Sakagami and K. Okamoto, *Chem. Lett.*, 1998, 201; (*c*) S. Decurtins, M. Gross, H. W. Schmalle and S. Ferlay, *Inorg. Chem.*, 1998, **37**, 2443.
13 E. F. Ullman, D. G. Osiecki, D. G. B. Boocock and R. Darcy, *J. Am. Chem. Soc.*, 1972, **94**, 7049.
14 (*a*) A. Caneschi, D. Gatteschi and P. Rey, *Prog. Inorg. Chem.*, 1991, **39**, 331 and references therein; (*b*) O. Kahn, *Molecular Magnetism*, VCH, New York, 1993; (*c*) E. Coronado, P. Dellhaès, D. Gatteschi and J. S. Miller (Editors), *Molecular Magnetism: From Molecular Assemblies to the Devices*, NATO ASI Series 321, Kluwer Academic Publishers, Dordrecht, 1996.
15 (*a*) T. Yoshida, T. Suzuki, K. Kanamori and S. Kaizaki, *Inorg. Chem.*, 1999, **38**, 1059; (*b*) T. Yoshida and S. Kaizaki, *Inorg. Chem.*, 1999, **38**, 1054; (*c*) T. Yoshida, K. Kanamori, S. Takamizawa, W. Mori and S. Kaizaki, *Chem. Lett.*, 1997, 603; (*d*) Y. Tsukahara, A. Iino, T. Yoshida, T. Suzuki and S. Kaizaki, *J. Chem. Soc., Dalton Trans.*, 2002, 181.
16 (*a*) Y. Yamamoto, T. Suzuki and S. Kaizaki, *J. Chem. Soc. Dalton Trans.*, 2001, 1566; (*b*) Y. Yamamoto, T. Suzuki and S. Kaizaki, *J. Chem. Soc. Dalton Trans.*, 2001, 2943.
17 (*a*) C. Benelli, A. Caneschi, D. Gatteschi, L. Pardi and P. Rey, *Inorg. Chem.*, 1990, **29**, 4223; (*b*) C. Benelli, A. Caneschi, D. Gatteschi and R. Sessoli, *Inorg. Chem.*, 1993, **32**, 4797.
18 C. Benelli, A. Caneschi, D. Gatteschi and L. Pardi, *Inorg. Chem.*, 1992, **31**, 741.
19 T. Akita, Y. Mazaki and K. Kobayashi, *J. Org. Chem.*, 1995, **60**, 2092.
20 (*a*) D. Luneau, P. Rey, J. Laugier, P. Fries, A. Caneschi, D. Gatteschi and R. Sessoli, *J. Am. Chem. Soc.*, 1991, **113**, 1245; (*b*) D. Luneau, P. Rey, J. Laugier, E. Belorizky and A. Cogne, *Inorg. Chem.*, 1992, **31**, 3578.
21 M. F. Richardson, W. F. Wagner and D. E. Sands, *J. Inorg. Nucl. Chem.*, 1968, **30**, 1275.
22 W. L. Busing and H. A. Levy, *Acta Crystallogr.*, 1957, **10**, 180.
23 (*a*) SIR-92, A. Altomare, M. C. Burla, M. Camalli, M. Cascarano, C. Giacovazzo, A. Guagliardi and G. J. Polidori, *Appl. Crystallogr.*, 1994, **27**, 435; (*b*) G. M. Sheldrick, SHELXL-97, Program for crystal determination and refinement, University of Göttingen, Germany, 1997.
24 Crystal Structure, Single Crystal Structure Analysis Software Package, Version 2.00, Rigaku and Molecular Structure Corporation, Japan, 2001.
25 M. G. B. Drew, *Coord. Chem. Rev.*, 1977, **24**, 179.
26 (*a*) C. Lescop, D. Luneau, E. Belorizky, P. Fries, M. Guillot and P. Rey, *Inorg. Chem.*, 1999, **38**, 5472; (*b*) A. Caneschi, A. Dei, D. Gatteschi, L. Sorace and K. Vostrikova, *Angew. Chem., Int. Ed.*, 2000, **39**, 246.
27 J.-P. Sutter, M. L. Kahn, S. Golhen, L. Ouahab and O. Kahn, *Chem. Eur. J.*, 1998, **4**, 571.
28 A. Caneschi, D. Gatteschi, A. Grand, J. Laugier, L. Pardi and P. Rey, *Inorg. Chem.*, 1988, **27**, 1031.
29 C. Lescop, D. Luneau, G. Bussière, M. Triest and C. Reber, *Inorg. Chem.*, 2000, **39**, 3740.
30 T. Isobe, S. Kida and S. Misumi, *Bull. Chem. Soc. Jpn.*, 1967, **40**, 1862.
31 M. Ogita, Y. Yamamoto, T. Suzuki and S. Kaizaki, *Eur. J. Inorg. Chem.*, in press.
32 W. DeW. Horrocks, Jr. and M. Albin, *Prog. Inorg. Chem.*, 1984, **31**, 1.
33 R. G. Lawrence, C. J. Jones and R. A. Kresinski, *J. Chem. Soc., Dalton Trans.*, 1996, 501.